distances in the bridging network.

The exchange coupling constant of -4.5 cm^{-1} that characterizes the superexchange interaction between the two terminal iron(III) ions is of special interest. As discussed above, attempts to fit the magnetic susceptibility data with this interaction being set to zero yielded unacceptable fits while those fits in which the exchange coupling constant was allowed to vary freely yielded results that matched the data very well. The filled out-of-plane copper(II) (d_{xz},d_{yz}) orbitals provide an effective superexchange pathway for the resultant antiferromagnetic interaction.

Exchange Coupling in [FeTPP][Cu(MNT)$_2$][FeTPP]. The electronic configuration of intermediate-spin $S = {}^3/_2$ iron(III) depends on the details of the coordination sphere of the iron. An electronic configuration of $(d_{xz,yz})^3(d_{xy})^1(d_{z^2})^1$ is frequently found, although the exact mutual placement of the one-electron energy levels depends on the ligand field strengths of the ligands and the details of the structure of the complex. In any event there are two unpaired electrons in out-of-plane orbitals and one unpaired spin in d_{xy}. There are several opportunities for superexchange interactions between the iron electrons and the unpaired electron in $d_{x^2-y^2}$ in $[Cu(MNT)_2]^{2-}$, and the sum of these interactions will determine the sign and magnitude of the iron–copper exchange coupling constant.

The pairwise interactions that contribute to J^{eff}_{Fe-Cu} are d_{z^2}(Fe)–$d_{x^2-y^2}$(Cu), d_{xz}(Fe)–$d_{x^2-y^2}$(Cu), and d_{xy}(Fe)–$d_{x^2-y^2}$(Cu). Of these, on the basis of the structural results for **2**, the interaction d_{z^2}(Fe)–$d_{x^2-y^2}$(Cu) is expected to be ferromagnetic while the other two pairwise orbital interactions are expected to be antiferromagnetic. Since $J^{eff}_{Fe-Cu}({}^3/_2,{}^1/_2)$ is nearly the same as $J^{eff}_{Fe-Cu}({}^1/_2,{}^1/_2)$, and since only the d_{xy}(Fe)–$d_{x^2-y^2}$(Cu) interaction is possible in the low-spin tail porphyrin (TPP-T) trimer, it may be concluded that the ferromagnetic d_{z^2}(Fe)–$d_{x^2-y^2}$(Cu) term and the antiferromagnetic d_{xz}(Fe)–$d_{x^2-y^2}$(Cu) term effectively cancel each other in [FeTPP][Cu(MNT)$_2$][FeTPP].

There are nine pairwise exchange interactions between the two terminal $S = {}^3/_2$ iron(III) ions, and on the basis of the mutual orientation of the magnetic orbitals, some of these are expected to be ferromagnetic in nature while others are expected to be antiferromagnetic. Perhaps the most important of the latter is d_{xz}(Fe)–$d_{\pm 1}$(Cu)–d_{xz}(Fe), the superexchange pathway identified above for [FeTPP-T][Cu(MNT)$_2$][FeTPP-T]. Since $|J^{eff}_{Fe-Fe}({}^3/_2,{}^3/_2)|$ is 30% greater than $|J^{eff}_{Fe-Fe}({}^1/_2,{}^1/_2)|$, it is clear that the sum of the other antiferromagnetic interactions dominates the sum of the ferromagnetic contributions. Although it is not possible to identify the individual orbital contributions that determine the effective exchange coupling constants, the comparison of these coupling constants for two complexes with similar structures but different spin states has permitted the selection of the predominant superexchange interactions.

Acknowledgment. This work was supported in part by the John Simon Guggenheim Memorial Foundation through a fellowship to W.E.H. and by the National Institutes of Health through Grant No. GM-30306 to C.M.E. W.E.H. thanks Professor Philipp Gütlich for his hospitality at Johannes Gutenberg Universität and Dr. A. B. Blake for helpful comments.

Registry No. **1**, 81534-76-1; **3**, 107985-43-3; Fe^{II}TPP, 16591-56-3; [TBA$^+$][Cu^{III}(MNT)$_2^-$], 19453-80-6; Fe^{II}TPP-T, 75529-04-3.

Contribution from the Department of Chemistry,
Iowa State University, Ames, Iowa 50011

Two Scandium Iodide Carbides Containing Dicarbon Units within Scandium Clusters: $Sc_6I_{11}C_2$ and $Sc_4I_6C_2$. Synthesis, Structure, and the Bonding of Dicarbon

Douglas S. Dudis and John D. Corbett*

Received November 14, 1986

The title compounds were synthesized from ScI_3, metal, and graphite at 850 °C in sealed niobium containers. Their structures were each refined in space group $P\bar{1}$ (for the two compounds, respectively: $Z = 2, 4$; $a = 10.046$ (3), 10.803 (3) Å; $b = 14.152$ (4), 13.959 (3) Å; $c = 9.030$ (3), 10.793 (4) Å; $\alpha = 104.36$ (3), 106.96°; $\beta = 110.45$ (2), 119.20 (3)°; $\gamma = 89.27$ (2), 87.80 (3)°; $R = 0.040$, 0.085; $R_w = 0.050$, 0.111). $Sc_6I_{11}C_2$ contains discrete M_6X_{12}-type clusters elongated along a pseudo-4-fold axis to accommodate the C_2 unit (d(C–C) = 1.39 (2) Å). The stoichiometry is achieved by bonding of clusters into pairs via four-coordinated I^{i-i} atoms. The phase $Sc_4I_6C_2$, which is of marginal stability, consists of infinite chains of condensed clusters each containing a C_2 unit, namely pairs of centric clusters of $\sim D_{2h}$ symmetry that are connected via shared metal edges by a distorted-trigonal-prismatic cluster. Extended Hückel calculations on $Sc_6I_{11}C_2$ indicate the principal bonding arises between cluster orbitals and π (e_u), π^* (e_g), and σ_s^* (a_{2u}) orbitals of C_2, with particularly strong bonding to the two metal atoms collinear with C_2 via the last two listed plus σ_p (a_{1g}). The HOMO in $Sc_6I_{11}C_2$ is the cluster-bonding $b_{2g}{}^1$ orbital, consistent with the measured magnetic susceptibility. Comparisons are made with the bonding in $Sc(Sc_6I_{12}C)$ and in other centered clusters.

Introduction

High-temperature studies of the metal-rich halides of scandium, yttrium, zirconium, and the lanthanide elements have revealed an extensive cluster chemistry exists in these systems. In addition, many of these compounds have been found to contain an "interstitial" element centered within each metal octahedron, and extended Hückel calculations have made it clear that this interstitial plays a major role in binding the cluster together. Scandium examples include $Sc(Sc_6Cl_{12}Z)$ and Sc_4Cl_6Z, Z = B, N,[1] and Sc_5Cl_8Z, Z = C, N.[2]

Recently, we reported[3] the first example of this type of chemistry for rare-earth-metal iodides with the synthesis and characterization of $Sc_7I_{12}C$, a compound that contains discrete but distorted $Sc_6I_{12}C$ clusters with a single carbon at each cluster center. It was noted at that time that $Sc_7I_{12}C$ is the most carbon-poor of such ternary iodides and that other, more carbon-rich, phases had been found. Herein we report the syntheses and characterization of two more, $Sc_6I_{11}C_2$ and $Sc_4I_6C_2$, both of which exhibit previously unknown compositions and structures. Interestingly, neither of these compositions has been recognized in extensive studies of the scandium–chlorine–carbon system.[1,2,4]

Both of the new compounds contain dicarbon units within scandium octahedra and thus represent a homologation from the single carbon in $Sc_7I_{12}C$. This interstitial moiety has already been found in gadolinium compounds such as $Gd_2Br_2C_2$,[5] $Gd_{10}Cl_{18}C_4$,[6]

(1) Hwu, S.-J.; Corbett, J. D. *J. Solid State Chem.* **1986**, *64*, 331.
(2) Hwu, S.-J.; Dudis, D. S.; Corbett, J. D. *Inorg. Chem.* **1987**, *26*, 469.
(3) Dudis, D. S.; Corbett, J. D.; Hwu, S.-J. *Inorg. Chem.* **1986**, *25*, 3434.
(4) Hwu, S.-J.; Corbett, J. D.; Poeppelmeier, K. R. *J. Solid State Chem.* **1985**, *57*, 43.
(5) Schwanitz-Schüller, U.; Simon, A. *Z. Naturforsch., B: Anorg. Chem., Org. Chem.* **1985**, *40B*, 710.

0020-1669/87/1326-1933$01.50/0

and $Gd_{12}I_{17}C_1$.[7] The first of these contains dicarbon units sandwiched between pairs of infinite metal layers, the second has discrete dicluster species in the form of pairs of gadolinium octahedra sharing a metal edge, the dicarbon units in each octahedraon being oriented normal to this edge and parallel to a pseudo-4-fold axis of the cluster, and the last has infinite zigzag chains of such condensed clusters. The title compounds are not only the first scandium compounds having dicarbon units in nominal octahedral clusters, but $Sc_6I_{11}C_2$ is the first discrete metal cluster containing dicarbon. This last feature allows a clearer look at the bonding of the dicarbon within the metal cluster using extended Hückel methods.

Experimental Section

The quality of the metal strips, ScI_3, and graphite used, the reaction procedures in sealed niobium tubes (~3 cm long), single-crystal and Guinier diffraction techniques, magnetic susceptibility measurement methods (SQUID), and the programs and parameters for crystallogaphic and extended Hückel calculations have been referenced or reported previously.[1-3] Unless noted othewise, reactions were run at 850 °C and the silica-jacketed containers than rapidly cooled to room temperature in air. Since ScI_3 and the reduced products decompose in the atmosphere, all manipulations were performed in a glovebox under a purified nitrogen or argon atmosphere. Single crystals were sealed in thin-walled capillaries.

$Sc_6I_{11}C_2$. The preparations of this compound and $Sc_4I_6C_2$ are best carried out such that the scandium strips are consumed in the reactions. Equilibrations of graphite with excess scandium strips and ScI_3 result in $Sc_7I_{12}C$ and Sc_xI_2 ($x \sim 0.9$),[3] the proportions depending on the amount of carbon used.

The first synthesis of $Sc_6I_{11}C_2$ was accomplished by heating Sc, ScI_3, and C in a 1:1:1 molar ratio for 2 weeks (251 mg of ScI_3, 7 mg of C), proportions that are in fact more appropriate to $Sc_4I_6C_2$. This gave a nicely crystalline black product with some crystals several millimeters on edge, and the specimen used in the crystallographic study was chosen from these. The powder pattern of the black (brown when ground) material showed that $Sc_6I_{11}C_2$ was the only iodide product.

Subsequently, this product was obtained in essentially quantitatve yield, probably via a vapor-phase transport reaction, after stoichiometric amounts of the reactants (~0.2-g scale) were allowed to react for 2 weeks. A few tiny crystals of ScI_3 that remained in the product were separated mechanically. The accuracy of the weights of the reactants was ~1 mg. To circumvent a possibly large relative error in the graphite weight, 2 g of an intimate mixture of 5.0 wt % graphite in ScI_3 was prepared, and the appropriate amount of this mixture was employed along with pure ScI_3 and Sc in later reactions.

$Sc_4I_6C_2$. This iodide forms in the most carbon-rich systems. Well-intergrown, black crystals of the phase were originally obtained along with some $Sc_6I_{11}C_2$ from a 1:1.2:2.2 mixture of Sc, ScI_3, and graphite (216 mg of ScI_3, 11 mg of C) that had been heated for 2 weeks. Following the crystal structure analysis, reactions run for 4 days–2 weeks with the 1:1:1 Sc:ScI_3:C stoichiometry indicated for the $Sc_4I_6C_2$ composition gave mainly $Sc_6I_{11}C_2$ with lesser amounts of $Sc_4I_6C_2$ being detected in some of the products. The use of excess graphite was later found to enhance the yield of $Sc_4I_6C_2$, and reactions with Sc:ScI_3:C proportions of 1:1.3:2.5 for 8 weeks at 710 °C or 1:1:2.8 for 2 weeks at 850 °C gave good yields although the former conditions did not give very good crystals. Reactions at 950 °C favor Sc_xI_2 as the product iodide.

Both the difficulties with the stoichiometric reactions and the need for excess carbon were resolved when it was noted that powder patterns of all of the microcrystalline products also showed broad lines of metal-deficient ScC (defect NaCl type[8]). Thus, the product sought must decompose at an appreciable rate at 850 °C according to

$$11Sc_4I_6C_2(s) \rightarrow 6Sc_6I_{11}C_2(s) \rightarrow 10Sc_{0.8}C(s)$$

and this can be repressed by the use of excess carbon. The $Sc_4I_6C_2$ is probably metastable but is accessible because of the low rate of formation of the monocarbide at these temperatures. Although transport of carbon clearly occurs in all of these syntheses, the species responsible is not known.

Crystallography. $Sc_6I_{11}C_2$. Four well-formed and visually single crystals of this phase were examined with a Syntex $P2_1$ four-circle diffractometer. Each crystal gave the same triclinic unit cell based on 15 reflections obtained from a random orientation rotation photographs. Axial photographs were excellent about *c*, but those along the *a* and *b* axes showed extra reflections at nonintegral lattice spacings. The first three crystals had a significant number of extra and relatively intense spots whereas the data crystal had only a few and these were quite weak. These observations suggest multiple and perhaps microtwinned crystals, but the effect was apparently insignificant in data collection. Similar results were obtained earlier with $Sc_7I_{12}C$,[3] although a nontwinned specimen was eventually found. Three-dimensional data were collected at room temperature with variable scan speeds (1.0–29.3° min^{-1}) and with no observable intensity decay. The data were empirically corrected for absorption (two ψ scans), Lorentz, and polariztion effects as before.[3]

Initial attempts to solve the structure with MULTAN in space group $P\bar{1}$ gave a solution with 24 close-packed iodines per cell but no room for the scandium atoms. The Patterson map clearly showed the pseudo-cubic-close-packed nature of the structure, which suggested the heavy-atom method might work, but all peaks in the resulting difference Fourier maps were ~2.3 Å from an iodine, similar to the MULTAN results. Finally, an iodine was placed at the origin in the space group *P*1, and a difference map was calculated. Only the largest peak from that map was added (as an iodine), and the coordinates of the second atom and the scale factor were refined. After many such iterations, the same model as before resulted. However, toward the latter stages the isotropic temperature factors of the iodine atoms were also varied. These became excessively large for two of the two iodine atoms, and a difference map revealed six scandium atoms ~2.3 Å from these particular atoms. Addition of these scandium atoms lowered the refinement indices dramatically and caused the temperature factors of the two pseudo-iodine atoms to increase to over 60 $Å^2$, at which point they were removed. A difference map showed dicarbon units actually occurred around these points, and these were added and successfully refined. Finally, the coordinates were transformed to correspond to $P\bar{1}$, and the structure was refined in the proper space group. The carbon atoms could not be refined anisotropically, as is usually the case with such compounds. Simultaneous refinement of the isotropic temperature factors and occupancies for carbon gave 0.9 (3) $Å^2$, 0.86 (5) and 1.3 (3) $Å^2$, 0.98 (5) for C(1) and C(2), respectively, so the carbon occupancies were subsequently fixed at unity. A final difference map was flat, the largest peak (<0.2 e $Å^{-3}$) being ~1.0 Å from an iodine. Other pertinent crystallographic information is given in Table I.

$Sc_4I_6C_2$. Crystals of $Sc_4I_6C_2$ were obtained from several reactions. The first batch were all multiple or twinned or both. However, one crystal had only a few small satellite crystals, and most reflections were free of interference, so diffraction data were collected from this specimen at room temperature with scan speeds between 2.0 and 29.3° min^{-1}. No decomposition was detected. The data were corrected for absorption

Table I. Crystallographic Data for $Sc_6I_{11}C_2$ and $Sc_4I_6C_2$

formula	$Sc_6I_{11}C_2$	$Sc_4I_6C_2$
fw	1689.7	965.3
space group	$P\bar{1}$	$P\bar{1}$
a, Å	10.046 (3)[a]	10.803 (3)[b]
b, Å	14.152 (4)	13.959 (3)
c, Å	9.030 (3)	10.793 (4)
α, deg	104.36 (3)	106.96 (3)
β, deg	110.45 (2)	119.20 (3)
γ deg	89.27 (2)	87.80 (3)
V, $Å^3$	1161.5 (6)	1348.4 (6)
Z	2	4
ρ(calcd), g cm^{-3}	4.83	4.75
cryst dimens, mm	0.20 × 0.30 × 0.25	0.20 × 0.20 × 0.25
μ(Mo Kα), cm^{-1}	161.2	154.9
trans coeff: min/max	0.26/0.87	0.47/0.81
refl measd[c]	$h,\pm k,\pm l$	$h,\pm k,\pm l$
2θ(max), deg	50	45
no. of refl collcd	4089	7299
no. of refl obsd	2566	4682
no. of unique refl ($I \geq 3\sigma(I)$)	2558	2383[d]
no. of params refined	163	198
R	0.040	0.085
R_w	0.050	0.111
GOF	1.01	1.04
largest residual (e $Å^{-3}$)	<0.2	<1.8
shift/error, last cycle	≤0.11	0.00

[a] These values were deduced from the diffractometer settings of 15 reflections with $20 < 2\theta < 25°$ and are within 1σ of those obtained from the Guinier powder pattern. [b] Deduced from 30 lines in the Guinier powder pattern. [c] At room temperature; Mo Kα radiation, λ = 0.71073 Å. [d] See text.

(6) Warkentin, E.; Masse, R.; Simon, A. *Z. Anorg. Allg. Chem.* **1982**, *491*, 323.
(7) Simon, A.; Warkentin, E. *Z. Anorg. Allg. Chem.* **1983**, *497*, 79.
(8) Rassaerts, H.; Nowotny, H.; Vinek, G.; Benosovsky, F. *Monatsh. Chem.* **1967**, *98*, 460.

based on four ψ scans at difference θ values and were further treated as above.

As with $Sc_6I_{11}C_2$, the Patterson map clearly showed the pseudo-close-packed nature of the iodine network. The structure was solved in the space group $P\bar{1}$ by assuming that certain peaks in a Patterson function were of the $2x$, $2y$, $2z$ type. Residual values were calculated separately for a number of the peaks so selected, those that were correctly identified typically being 5% lower, and a difference map was calculated for the best group. Iterations similar to those employed above were used, and the results converged quickly to the solution reported herein.

A difference map computed after the iodine and scandium atoms had been refined isotropically clearly revealed the carbon atoms, and their introduction lowered the R indices ~1.5%. The iodines could then be refined anisotropically, but a few of the scandium atoms gave distorted ellipsoids and the refinement stopped at $R \sim 8.5\%$, $R_w \sim 14\%$. An examination of the data revealed that all reflections with poor agreement had positive values of δ [$=(|F_o| - |F_c|)/(\sigma_F \times \mathrm{GOF})$]. Both this and the problems associated with the scandium atoms appeared attributable to interference from satellite reflections. Otherwise, the structure at this point made chemical sense in terms of bond lengths and angles, and the anisotropic iodine and isotropic scandium thermal parameters were quite normal.

No better specimen could be found after more syntheses and the examination of ~15 other $Sc_4I_6C_2$ specimens, although observed vs. calculated powder patterns made it clear that we were always dealing with the same phase. There are several factors at play here. One is that chain structures are often inherently difficult to crystallize well.[9] This can be overcome by increasing reaction/annealing times. However, this is not practical in the present case since the compound appears to be metastable, or at least marginally stable, with respect to $Sc_6I_{11}C_2$ and Sc_xC (above). Additionally, the crystals always seemed to be intergrown and to require cleaving. The $Sc_6I_{11}C_2$ that forms as a decomposition product gives much nicer but otherwise visually indistinguishable crystals.

Given the above problems, we decided to reexamine the original data crystal. A second data set was collected, but each reflection was now measured three times at ψ = 0, 20, and 40° except where limited by diffractometer angles. The data were recorded as above, and refinement was continued to R = 9.7%, R_w = 14.8%, and GOF = 3.07 (2423 reflections). This time only B_{33} of Sc(5) was abnormally small, but the C(4)–C(4) distance was short, ~1.1 Å. As before, examination of F_o and F_c revealed large positive values for δ. Since the magnitude of the most positive δ should be about the same as that of the most negative δ for random errors, the 40 reflections with $\delta > 2|-\delta_{max}|$, where $-\delta_{max}$ is the most negative δ, were eliminated from the data set. Normally, removing bad data does not alter the parameters determined with the remaining data, but it does improve the precision. In this case, however, the unreasonable parameters showed a marked improvement, though the C(4)–C(4) was still short. At this stage, the isotropic temperature factors for three of the four carbon atoms could be refined for the first time; that for C(2) still had to be fixed (at 1.1 Å^2, the average of the others) but the occupancy could be refined (1.44 (8)). Thus, there were still enough bad reflections in the data set to give some problems; 115 of the 124 reflections remaining with $|\delta| > 2.0$ had positive values of δ. An examination of the data showed almost no variation of R and R_w with 2θ, but many of the bad reflections were in a small region of F_o. Reweighting of the data grouped as a function of F_o lowered R_w by 0.4%. The final crystallographic results are summarized in Table I. The largest residual density, <1.8 e Å^{-3}, was ~1 Å from an iodine.

Most of the 40 reflections eliminated were in a ~30° range in χ and ϕ (or a symmetry equivalent thereof). Others just outside this range had very skewed peak profiles. Hence, only one section of the data was affected to any great extent, which is probably why the structure could be solved. Refinements with other defensible elimination schemes did not improve matters. In the end, a fairly normal treatment with a minor excision of 1.6% of the data on a statistically meaningful criterion proved as good as any other procedure. Although the standard deviations of the structural parameters and interatomic distances are 2–4 times that for the first phase reported here, the structure is certainly sufficiently defined to relate and compare.

Results and Discussion

$Sc_6I_{11}C_2$. The atomic coordinates for this structure are given in Table II, and important interatomic distances, in Table III. Thermal parameters and angular data are available as supplementary material. As noted earlier, the iodines are nearly close packed in this structure. There is also a pseudosymmetry operation such that atoms I(n + 5), $2 \le n \le 6$, occur at about x, $^1/_2 + y$, z from I(n) at x, y, z, with I(1) excluded because the cluster is centered about the site where that atom would occur. These factors together with the predominance of the scattering by iodine atoms account for much of the initial difficulty in solving the structure.

Table II. Atomic Coordinates for $Sc_6I_{11}C_2$

atom	x	y	z
I(1)	0.2989 (1)	0.27403 (8)	0.3801 (1)
I(2)	0.5531 (1)	0.14964 (7)	0.1227 (1)
I(3)	0.3744 (1)	0.06368 (7)	0.6284 (1)
I(4)	0.2105 (1)	0.47739 (8)	0.1198 (1)
I(5)	0.03815 (9)	0.39242 (7)	0.6175 (1)
I(6)	0.8745 (1)	0.30818 (7)	0.1290 (1)
I(7)	0.5335 (1)	0.64892 (7)	0.1341 (1)
I(8)	0.3729 (1)	0.56411 (8)	0.6189 (1)
I(9)	0.2169 (1)	0.97948 (8)	0.1401 (1)
I(10)	0.0487 (1)	0.89689 (7)	0.6227 (1)
I(11)	0.8806 (1)	0.81650 (7)	0.1239 (1)
Sc(1)	0.4759 (3)	0.1204 (2)	0.3861 (3)
Sc(2)	0.7794 (2)	0.2661 (2)	0.4308 (3)
Sc(3)	0.5775 (2)	0.3589 (2)	0.6214 (3)
Sc(4)	0.6531 (3)	0.2043 (2)	0.8290 (3)
Sc(5)	0.8471 (3)	0.1070 (2)	0.6316 (3)
Sc(6)	0.9494 (3)	0.3489 (2)	0.8603 (3)
C(1)	0.344 (1)	0.797 (1)	0.432 (2)
C(2)	0.227 (1)	0.738 (1)	0.314 (2)

Table III. Bond Lengths (Å) in $Sc_6I_{11}C_2$

Sc(1)–Sc(2)	3.550 (4)	Sc(2)–Sc(6)	3.535 (3)
Sc(1)–Sc(3)	3.459 (4)	Sc(3)–Sc(4)	3.143 (3)
Sc(1)–Sc(4)	3.647 (3)	Sc(3)–Sc(6)	3.625 (4)
Sc(1)–Sc(5)	3.643 (4)	Sc(4)–Sc(5)	3.164 (3)
Sc(2)–Sc(3)	3.171 (3)	Sc(4)–Sc(6)	3.523 (4)
Sc(2)–Sc(5)	3.154 (3)	Sc(5)–Sc(6)	3.484 (4)
Sc(1)–I(1)	2.790 (3)	Sc(4)–I(2)	3.396 (3)
Sc(1)–I(2)	2.866 (3)	Sc(4)–I(3)	3.145 (3)
Sc(1)–I(3)	2.987 (3)	Sc(4)–I(6)	2.888 (3)
Sc(1)–I(3)′	2.989 (3)	Sc(4)–I(7)	2.817 (3)
Sc(1)–I(9)	3.094 (3)	Sc(4)–I(9)	2.926 (3)
Sc(2)–I(2)	3.004 (3)	Sc(5)–I(3)	3.158 (3)
Sc(2)–I(5)	2.891 (3)	Sc(5)–I(9)	2.891 (3)
Sc(2)–I(6)	3.367 (2)	Sc(5)–I(10)	2.826 (3)
Sc(2)–I(8)	2.878 (3)	Sc(5)–I(10)′	3.577 (3)
Sc(2)–I(10)	2.909 (3)	Sc(5)–I(11)	2.863 (3)
Sc(3)–I(1)	2.924 (3)	Sc(6)–I(4)	2.922 (3)
Sc(3)–I(4)	3.054 (3)	Sc(6)–I(4)′	3.065 (3)
Sc(3)–I(7)	2.824 (2)	Sc(6)–I(5)	2.834 (3)
Sc(3)–I(8)	2.844 (3)	Sc(6)–I(6)	2.960 (3)
Sc(3)–I(8)′	3.536 (3)	Sc(6)–I(11)	2.882 (3)
C(1)–Sc(1)	2.09 (1)	C(2)–Sc(2)	2.35 (1)
C(1)–Sc(2)	2.35 (1)	C(2)–Sc(3)	2.37 (1)
C(1)–Sc(3)	2.33 (1)	C(2)–Sc(4)	2.33 (1)
C(1)–Sc(4)	2.36 (1)	C(2)–Sc(5)	2.30 (1)
C(1)–Sc(5)	2.32 (1)	C(2)–Sc(6)	2.07 (1)
C(1)–C(2)	1.39 (2)		

The structure of $Sc_6I_{11}C_i$ consists of discrete Sc_6I_{12}-type octahedral clusters that have been elongated along a pseudo-4-fold axis to accommodate a C_2 unit with that orientation, as illustrated in Figure 1. Also shown are the edge-bridging iodine atoms (I^i) in neighboring clusters that serve the evidently essential feature of bonding at the terminal positions (I^a) in this cluster and so are represented as $I^{a\text{-}i}$. A second unusual feature of the structure is the presence of pairs of four-coordinate iodine(3) atoms that are edge-bridging in two clusters, that is, $I^{i\text{-}i}$. As shown in Figure 2, this functionality generates a pair of clusters linked by four bridges, two $I^{i\text{-}i}$ and two $I^{i\text{-}a}$, that are arranged about an inversion center between the clusters. The remaining intercluster interactions involve five $I^{i\text{-}a}$-type bonds. Although full details have not been published, what appears to be similar intercluster connections in $Gd_{10}I_{16}(C_2)_2$ link pairs of condensed clusters into infinite chains.[10,11]

(9) Poeppelmeier, K. R.; Corbett, J. D. *Inorg. Chem.* **1977**, *16*, 1107.

(10) See Figure 4c in ref 11 for a picture of $Gd_{10}I_{16}C_4$.
(11) Simon, A. *J. Solid State Chem.* **1985**, *57*, 2.

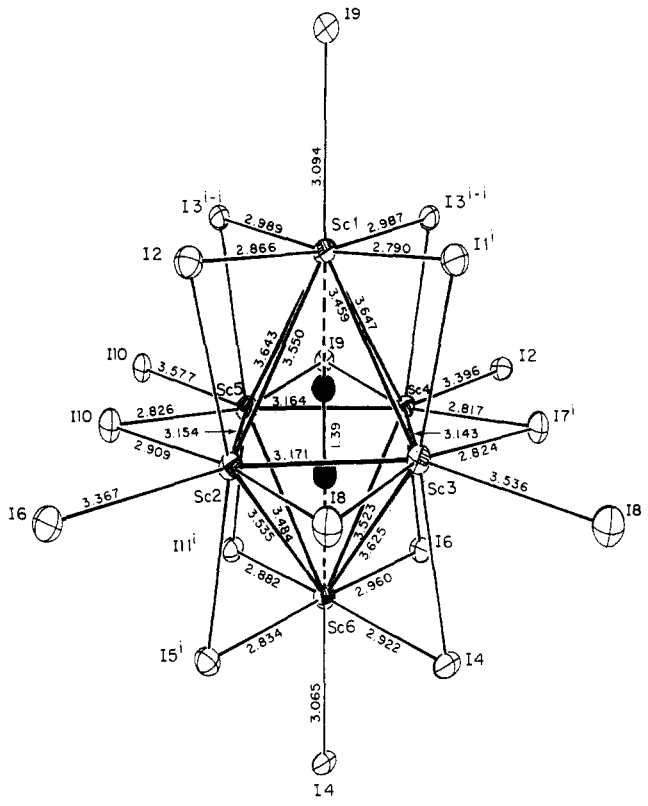

Figure 1. A single cluster unit of $Sc_6I_{11}C_2$ together with intercluster bridging atoms (ORTEP, 50% probability thermal ellipsoids). Bridging iodine atoms with no superscripts are two-coordinate, those with i are three-coordinate I^{i-a}, and $I(3)^{i-i}$ is four-coordinates.

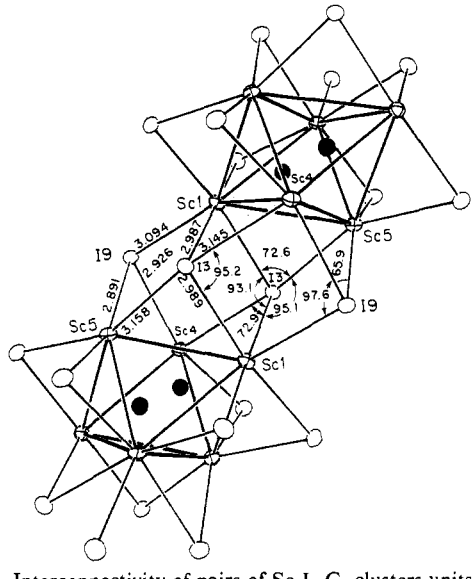

Figure 2. Interconnectivity of pairs of $Sc_6I_{11}C_2$ clusters units via four-coordinate $I(3)^{i-i}$ and three-coordinate $I(9)^{i-a}$.

The orientation of the C_2 unit in the latter with respect to the halogen bridge is different, however. Intercluster connections involving single X^{i-i} bridges are also found in $Gd_{10}Cl_{18}(C_2)_2$[6] and $KZr_6Cl_{13}Be$.[12]

The cluster may be represented as $Sc_6(C_2)I^i{}_4I^{i-i}{}_{2/2}I^{i-a}{}_{6/2}I^{a-i}{}_{6/2}$, where iodine atoms 1, 5, 7, and 11 are only edge-bridging I^i, atoms 2, 4, 6, 8, 9, and 10 are dual functional, I^{i-a} here and I^{a-i} elsewhere, and the unusual atom 3 is I^{i-i}. As expected, the Sc–I^i distances increase with coordination number of the iodine, these ranging from 2.79–2.88 Å in the first group to 2.99 Å in the last when the effects of cluster elongation are ignored. The equator of the cluster about the π system of the C_2 unit exhibits fairly uniform Sc–Sc distances of 3.14–3.17 Å, appreciably less than an average for the 12 edges of 3.26 Å in $Sc(Sc_6I_{12}C)$,[3] 3.27 Å in Sc_7Cl_{10},[9] and 3.24 Å in $Sc_7Cl_{10}C_2$[7] where isolated carbon atoms occur in double chains of condensed octahedra. The shorter Sc–Sc distances will be seen to arise not from stronger Sc–Sc bonding but from the maintenance of approximately constant Sc–C distances. On the other hand, distances from the equatorial metals to the apical Sc(1) and Sc(6) atoms are significantly greater, 3.46–3.65 Å, because of the dimensional requirements of the C_2 unit.

The fairly uniform Sc–C separations in $Sc_7I_{12}C$ and $Sc_7Cl_{10}C_2$, 2.30 and 2.31 Å, respectively, are similar to the average of the eight about the waist of the C_2 units here, 2.34 Å. However, a noteworthy aspect of this structure is that the Sc–C distances between the ends of the dicarbon and the apical metal atoms are 2.08 Å, 0.26 Å shorter than the others. The shortening is still 0.22 Å or more when comparison is made with the uniform Sc–C distances in $Sc_7I_{12}C$[3] or the average in $Sc_7Cl_{12}(B,N)$,[1] both examples having only single interstitial atoms in each cluster. The same difference still pertains when data for a considerable number of zirconium cluster halide monocarbides[12-14] are considered along with a small correction for the difference in metal core sizes (crystal radii[15]). This unusual feature in $Sc_6I_{11}C_2$ must reflect a particularly strong axial bonding of the C_2 unit within the metal cluster, as will be considered later.

Structures found for a wide variety of cluster compounds generally represent fairly efficient ways of packing these units while at the same time finding means whereby halide from other clusters bond at the cluster vertices, often via double-function atoms such as I^{i-a}. The present structure demonstrates that this factor is more important than achieving uniform metal–halogen bonding and halogen basicity since the compound contains two-, three-, and four-coordinate iodine atoms in I^i, I^{i-a}, and I^{i-i}, respectively. Distances between scandium and the terminal iodine atoms I^{a-i} show a very wide range, 3.06–3.58 Å, although it will be noted that four occur in the 3.37–3.58 Å range while the distinctively short pair near 3.08 Å again involve bonds to Sc(1) and Sc(6) and lie on the axis along which the cluster is elongated.

The seemingly short axial scandium–terminal iodine distances are probably relatively normal and arise from a greatly diminished matrix effect[16] at these points. In many such clusters the optimal dimensions for metal–metal and metal–interstitial bonding are not consistent with the greater size of the edge-bridging halide. As a result the halide are forced outward from the ideal positions, at the same time suffering some loss of bonding to the smaller metal framework, and the metal atoms are observed to lie well inside of the plane of the four adjacent edge-bridging halides (Figure 1). In the present structure this is reflected in the angles on these faces involving diagonally opposed iodines about the vertex metal, e.g., I(7)–Sc(3)–I(8). These lie between 153 and 159° for scandium atoms 2–5 about the cluster equator. On the other hand, angles at the axial metal atoms that have in effect been forced outward by the dicarbon exhibit are 171–176°. Thus, the approach of the intercluster bridging I^a atoms to the former type of metal vertex is in turn clearly restricted by I^a–I^i contacts, which average 4.05–4.11 Å at the equatorial Sc(2)–Sc(5) atoms. Correspondingly, I^a atoms at the less hindered axial vertices not only approach the metal much more closely but also exhibit slightly larger closed-shell contact distances, 4.14 and 4.19 Å (supplementary material). Thus the shorter Sc–I^a distances at the latter probably represent more nearly "normal" bonds.

The stoichiometry of $Sc_6I_{11}C_6$ indicates that there should be an odd number of electrons (15) available for Sc–Sc and Sc–C bonding. Figure 3 shows the reciprocal molar magnetic susceptibility for a 70 ± 2 mg sample as a function of temperature. A Curie–Weiss relationship with a consistent value of μ = 1.8 (1)

(12) Ziebarth, R. P.; Corbett, J. D. *J. Am. Chem. Soc.* **1985**, *107*, 4571.

(13) Smith, J. D.; Corbett, J. D. *J. Am. Chem. Soc.* **1985**, *107*, 5704.
(14) Ziebarth, R. P.; Corbett, J. D., unpublished research.
(15) Shannon, R. D. *Acta Crystallogr., Sect. A: Cryst. Phys., Diffr. Theor. Gen. Crystallog.* **1976**, *A32*, 751.
(16) Corbett, J. D. *J. Solid State Chem.* **1981**, *37*, 335.

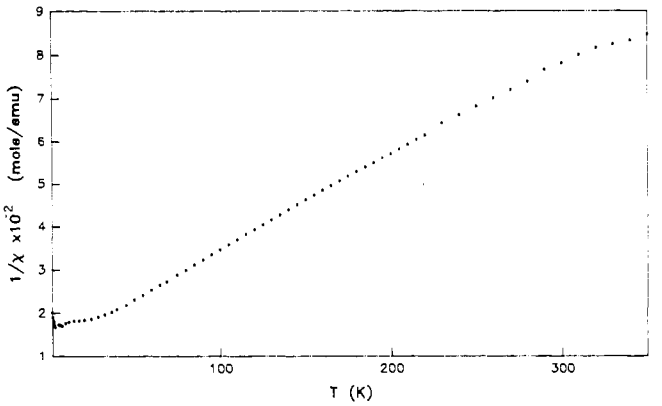

Figure 3. Reciprocal magnetic susceptibility of $Sc_6I_{11}C_2$ as a function of temperature (K).

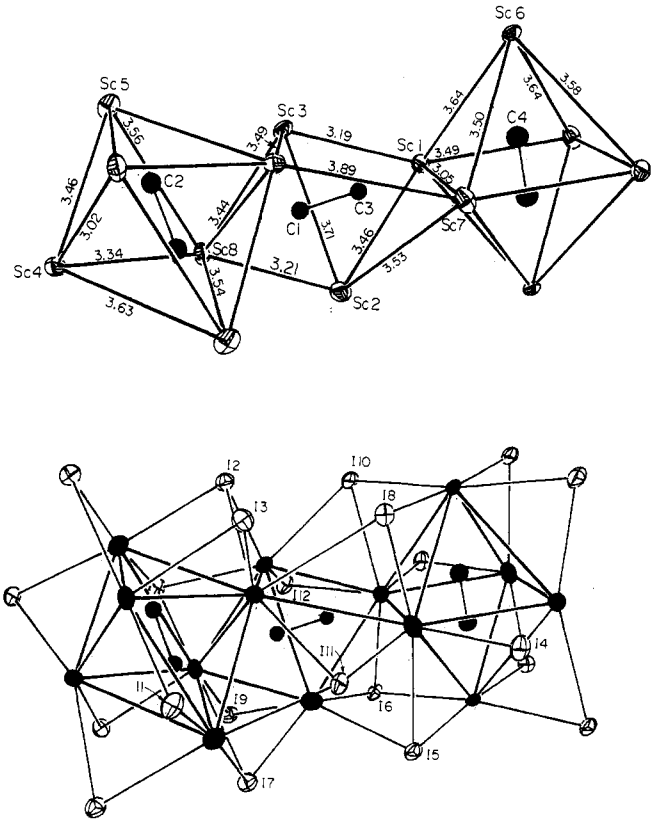

Figure 4. Top: Slightly more than the independent unit of scandium cluster units in $Sc_4I_6C_2$ (ORTEP, 50% probability). The outer pair of clusters are centric. Bottom: The top unit with iodine atoms added and the metal and carbon atoms darkened.

μ_B fits over the central range. Some intercluster coupling may occur at low temperatures.

$Sc_4I_6C_2$. Atomic coordinates for the atoms in this compound are given in Table IV, and important bond lengths, in Table V. The thermal parameters and bond angle data are available as supplementary material. This compound contains an unusual infinite chain of edge-sharing Sc_6I_{12}-type units with a dicarbon in each, the independent unit being $Sc_8I_{12}C_4$. The top part of Figure 4 shows somewhat more than the repeat fragment while the view at the bottom shows the same unit with the iodines added. The chains run diagonally through the triclinic cell with the left- and right-hand clusters in Figure 4 centered on the inversion points 0, 0, 0 and $^1/_2$, $^1/_2$, and $^1/_2$, respectively. The centric clusters can be approximated as D_{2h} in symmetry, for not only are they elongated to accommodate the dicarbon unit but the shared metal edges are characteristically shortened to 3.02 and 3.05 Å while the other equatorial Sc–Sc separations are increased relative to those in $Sc_6I_{11}C_2$. Equatorial–apex distances in the metal clusters

Table IV. Atomic Coordinates for $Sc_4I_6C_2$

atom	x	y	z
Sc(1)	0.4369 (7)	0.3981 (6)	0.5981 (9)
Sc(2)	0.0716 (8)	0.3398 (6)	0.3570 (9)
Sc(3)	0.3371 (8)	0.1611 (6)	0.4734 (9)
Sc(4)	0.1946 (7)	0.1085 (6)	0.0897 (9)
Sc(5)	0.8455 (8)	0.1219 (6)	0.8344 (8)
Sc(6)	0.7032 (7)	0.3770 (5)	0.4805 (8)
Sc(7)	0.3375 (8)	0.3949 (6)	0.2795 (9)
Sc(8)	0.9845 (8)	0.1004 (6)	0.1964 (9)
I(1)	0.1432 (3)	−0.0012 (2)	0.4303 (3)
I(2)	0.4256 (3)	0.0037 (2)	0.2885 (3)
I(3)	0.2744 (3)	0.0054 (2)	0.8675 (3)
I(4)	0.3621 (3)	0.4948 (2)	0.0924 (3)
I(5)	0.0730 (3)	0.4961 (2)	0.2233 (3)
I(6)	0.2102 (3)	0.5025 (2)	0.6482 (3)
I(7)	0.7961 (3)	0.2523 (2)	0.0663 (3)
I(8)	0.4982 (3)	0.2412 (2)	0.1933 (3)
I(9)	0.9389 (3)	0.2469 (2)	0.4765 (3)
I(10)	0.6554 (3)	0.2457 (2)	0.6260 (3)
I(11)	0.0905 (3)	0.2581 (2)	0.9283 (3)
I(12)	0.3703 (3)	0.2617 (2)	0.7517 (3)
C(1)	0.171 (4)	0.209 (3)	0.287 (4)
C(2)	0.048 (3)	−0.030 (2)	0.047 (3)
C(3)	0.279 (4)	0.290 (3)	0.386 (4)
C(4)	0.550 (4)	0.474 (3)	0.512 (5)

Table V. Bond Lengths (Å) in $Sc_4I_6C_2$

Sc(1)–Sc(2)	3.46 (1)	Sc(3)–Sc(8)	3.44 (1)
Sc(1)–Sc(3)	3.19 (1)	Sc(4)–Sc(5)	3.46 (1)
Sc(1)–Sc(6)	3.58 (1)	Sc(4)–Sc(5)′	3.63 (1)
Sc(1)–Sc(6)′	3.64 (1)	Sc(4)–Sc(7)	3.89 (1)
Sc(1)–Sc(7)	3.05 (1)	Sc(4)–Sc(8)	3.02 (1)
Sc(1)–Sc(7)′	3.35 (1)	Sc(4)–Sc(8)′	3.34 (1)
Sc(2)–Sc(3)	3.71 (1)	Sc(5)–Sc(8)	3.54 (1)
Sc(2)–Sc(7)	3.53 (1)	Sc(5)–Sc(8)′	3.56 (1)
Sc(2)–Sc(8)	3.21 (1)	Sc(6)–Sc(7)	3.50 (1)
Sc(3)–Sc(4)	3.49 (1)	Sc(6)–Sc(7)′	3.64 (1)
Sc(1)–I(4)	2.893 (8)	Sc(5)–I(1)	2.922 (8)
Sc(1)–I(6)	2.995 (8)	Sc(5)–I(2)	2.941 (8)
Sc(1)–I(10)	3.080 (8)	Sc(5)–I(7)	2.903 (8)
Sc(1)–I(12)	3.162 (8)	Sc(5)–I(10)	3.122 (8)
Sc(2)–I(5)	2.950 (8)	Sc(5)–I(11)	2.880 (8)
Sc(2)–I(6)	2.963 (9)	Sc(6)–I(5)	2.948 (8)
Sc(2)–I(6)′	3.675 (8)	Sc(6)–I(6)	2.896 (8)
Sc(2)–I(7)	3.021 (8)	Sc(6)–I(8)	2.881 (8)
Sc(2)–I(9)	2.885 (8)	Sc(6)–I(9)	3.081 (7)
Sc(3)–I(1)	2.921 (8)	Sc(6)–I(10)	2.939 (8)
Sc(3)–I(2)	2.978 (8)	Sc(7)–I(4)	2.880 (9)
Sc(3)–I(2)′	3.878 (8)	Sc(7)–I(5)	3.004 (8)
Sc(3)–I(10)	3.096 (8)	Sc(7)–I(8)	2.933 (8)
Sc(3)–I(12)	2.765 (9)	Sc(7)–I(11)	3.381 (9)
Sc(4)–I(2)	3.049 (8)	Sc(8)–I(1)	3.000 (8)
Sc(4)–I(3)	2.911 (8)	Sc(8)–I(3)	2.885 (8)
Sc(4)–I(8)	3.334 (7)	Sc(8)–I(7)	3.038 (8)
Sc(4)–I(11)	2.947 (8)	Sc(8)–I(9)	3.367 (8)
C(1)–Sc(2)	2.21 (4)	C(3)–Sc(1)	2.19 (4)
C(1)–Sc(3)	2.21 (4)	C(3)–Sc(2)	2.22 (4)
C(1)–Sc(4)	2.31 (4)	C(3)–Sc(3)	2.20 (4)
C(1)–Sc(8)	2.19 (4)	C(3)–Sc(7)	2.37 (4)
C(2)–Sc(4)	2.34 (3)	C(4)–Sc(1)	2.28 (4)
C(2)–Sc(4)′	2.40 (3)	C(4)–Sc(1)′	2.47 (7)
C(2)–Sc(5)	2.01 (3)	C(4)–Sc(6)	2.19 (4)
C(2)–Sc(8)	2.37 (3)	C(4)–Sc(7)	2.24 (4)
C(2)–Sc(8)′	2.38 (3)	C(4)–Sc(7)′	2.40 (4)
C(1)–(3)	1.40 (5)	C(4)–C(4)′	1.24 (8)
C(2)–(2)′	1.48 (5)		

are very similar to those already described in both range and average. Although the crystallography did not locate the lighter atoms in this structure as precisely, the average of the three C–C distances and the averages of both types of Sc–C distances in the centric clusters are all very close to those found in $Sc_6I_{11}C_2$.

The third, interconnecting cluster is more novel. The view in Figure 4 might first be thought to represent a distorted octahedron, but some disproportionately long Sc–Sc distances and the orien-

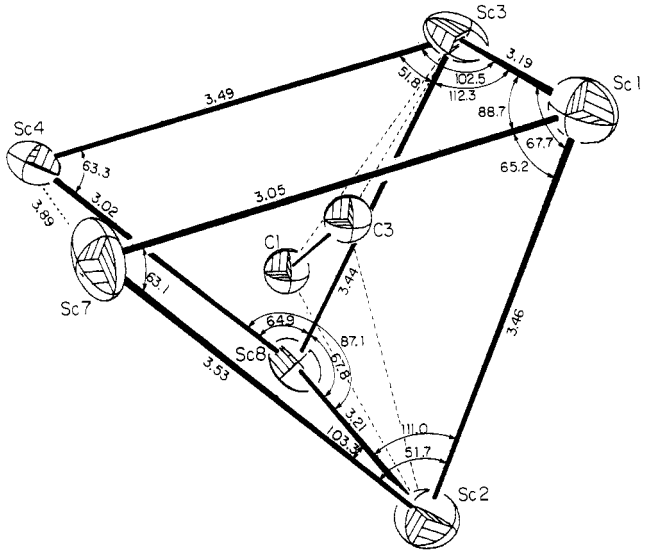

Figure 5. Another view of the pseudo trigonal prism that interconnects the left- and rightmost octahedral clusters in Figure 4. The edges shared with the neighboring clusters are the shorter Sc(1)–Sc(7) and Sc(4)–Sc(8).

tation of the C_2 unit (toward the reader from Sc(1) and Sc(8) in the figure) suggest other descriptions are better. One is that the shared edges of the centric clusters, Sc(4)–Sc(8) and Sc(1)–Sc(7), are bridged by Sc(3) and Sc(2) atoms, respectively, at distances of 3.44–3.53 Å, and each of these bridging atoms is also well bonded (3.19, 3.21 Å) to one end of the other edge. Another view in Figure 5, approximately normal to that in Figure 4, shows more clearly that the C_2 enclosure is better described as a distorted trigonal prism with triangular faces defined by these shared edges and the bridging Sc(3) and Sc(2) atoms, respectively. The C_2 unit is oriented approximately toward the centers of the Sc(4)–Sc(8) and Sc(1)–Sc(7) edges that are shared with the octahedra, with Sc–C distances of 2.19 Å (Sc(8)) and 2.31 Å (Sc(4)) from C(1) and 2.19 Å (Sc(1)) and 2.37 Å (Sc(7)) from C(3). Interestingly, the intercluster bridging Sc(2) and Sc(3) atoms are now seen to be quite uniformly placed with respect to the C(1)–C(3) π system. The four Sc–C distances here lie in the range of 2.20–2.22 Å and generate the butterfly-shaped arrangement outlined by dashes in the figure.

As might be expected with such a series of condensed clusters, the scandium–iodine bonding about the chain shown in the bottom of Figure 4 is diverse, with a range of both distances (2.77–3.38 Å) and, again, coordination numbers (2–4) for the iodine. The unusual bridging Sc(2) and Sc(3) atoms are each well bonded to four iodines within the chain, a factor that is doubtlessly important in the stability of this configuration. In addition, fairly short (3.08, 3.12 Å) interchain Sc–$I^{a\text{-}i}$ bridges approximately collinear with the C_2 units in the two centric clusters again interlink these at Sc(5) and Sc(6), a feature similar to that found in $Sc_6I_{11}C_2$ (Figure 1).

In comparison, this structure is only distantly related to the infinite zigzag cluster chains found in $Gd_{12}I_{17}(C_2)_3$.[7] In the latter, distorted clusters condensed in pairs analogous to those in $Gd_{10}Cl_{18}(C_2)_2$[5] and with C_2 units perpendicular to the shared edge are joined at nontrans edges by another like unit with the C_2 unit oriented normal to those in the dimer. Perhaps more relevant are the structures reported[8,17] for the most carbon-rich scandium carbides, Sc_2C_3 and $Sc_{15}C_{19}$, as these appear to contain carbon environments somewhat analogous to those found in various scandium iodides. The first contains C_2 units in the Pu_2C_3 structure according to powder data.[8] Although some details are not given, a single-crystal study ($R = 0.15$) of $Sc_{15}C_{19}$[17] yielded a structure with highly condensed and distorted scandium octahedra that contain either C or C_2 ($d = 1.25$ Å) interstitial units. The shorter Sc–C distances found were comparable to those reported here, 2.24–2.48 Å.

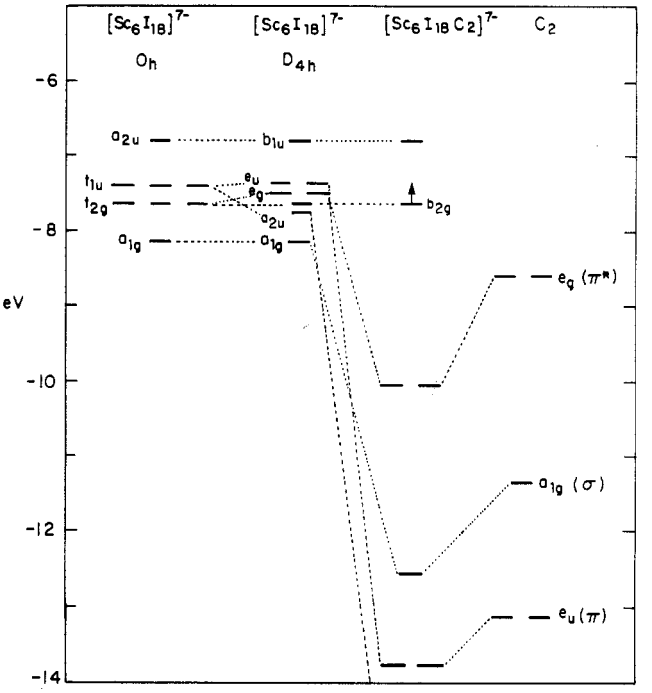

Figure 6. Molecular orbital diagram for $Sc_6I_{11}C_2$ from extended Hückel calculations together with the Sc–Sc bonding levels in the empty $[Sc_6I_{18}]^{7-}$ cluster (O_h and D_{4h} symmetries) and the isolated C_2 unit. The HOMO is b_{2g}^1. (Omitted for clarity are the primarily I 5s and 5p orbitals, the low lying σ_s and σ_s^* from C_2, and all antibonding levels.)

Molecular Orbital Calculations. Several MO investigations on compounds containing dicarbon units within edge-shared Gd_6X_{12}-type clusters have been reported.[18-21] All of these utilized band methods more familiar to the solid state and presented the results in terms of densities of states and their projections. The $Sc_6I_{11}C_2$ structure is simpler in that it provides dicarbon in a discrete M_6X_{12}-type cluster, and so the bonding can be described in more molecular-like terms. It should be noted that these solid-state structures always include intercluster-bridging halides at the vertices of every octahedron, and as has been shown for Zr_6I_{12}-C-type clusters in a number of structures,[13] careful treatments of the electronic structures of such clusters should include these terminal atoms in the model. The orbital and atom parameters utilized in the extended Hückel calculations are included in the supplementary material.

The left side of Figure 6 shows an energy diagram of such an idealized $(Sc_6I_{12})I_6^{7-}$ unit in octahedral symmetry and, following, the result of the axial elongation to a D_{4h} model with distances appropriate to the observed structure. The lowest seven metal-based cluster orbitals in the O_h (D_{4h}) idealization are shown: these occur with a_{1g} (a_{1g}), t_{1u} (e_u, a_{2u}), and t_{2g} (e_g, b_{2g}) representations. The low-lying iodine 5s functions and iodine 5p nonbonding pairs intermixed with iodine–scandium bonds have been omitted for clarity; these occur in blocks at energies between −18.7 and −18.5 eV and between −13.6 and −12.1 eV, respectively. On the right side of the figure are the important valence orbitals for C_2 calculated at the observed distance, 1.39 Å. The lower lying of the eight valence orbitals on the C_2 fragment, a_{1g} (nominally σ_g (2s)) and a_{2u} (σ_u^*—lone pair), as well as the topmost a_{2u}^* are not shown as they were calculated to be well isolated energetically from the

(17) Jedlicka, H.; Nowotny, H.; Benesovsky, F. *Monatsh. Chem.* **1971**, *102*, 389.
(18) Satpathy, S.; Anderson, O. K. *Inorg. Chem.* **1985**, *24*, 2604.
(19) Bullett, D. W. *Inorg. Chem.* **1985**, *24*, 3319.
(20) The π_g and π_u designations of the dicarbon states in $Gd_{10}Cl_{18}C_4$ have been reversed in ref 19.
(21) Miller, G. J.; Burdett, J. K.; Schwarz, C.; Simon, A. *Inorg. Chem.* **1986**, *25*, 4437.
(22) Pearson, W. B. *The Crystal Chemistry and Physics of Metals and Alloys*; Wiley-Interscience: New York, 1972; p 151.

Table VI. Reduced Scandium–Dicarbon Overlap Populations in Bonding Orbitals in $Sc_6I_{11}C_2$ according to Symmetry and Scandium Type

dicarbon orbital type	approx energy, eV	no.[a]	% C	scandium atoms[b] equatorial (×4)	scandium atoms[b] axial (×2)	tot.
π^* (e_g)	−10.0	2	58	0.171	0.138	0.958
σ_p (a_{1g})	−12.5	2	32, 35	−0.012	0.124	0.203
π (e_u)	−13.6	6	32, 23, 22	0.154	0.027	0.672
σ_s^* (a_{2u})	−18.0	3	53, 21, 6	0.031	0.207	0.537
σ_s (a_{1g})	−26.3	1	98	−0.008	0.027	0.025
other (a_{1g}, e_u)				0.026	0.052	0.210
tot. overlap pop./metal atom				0.363	0.576	

[a] The number of orbitals that provide major contributions for that symmetry. [b] $c_i c_j S_{ij}$ for each Sc–C_2 interaction summed over relevant orbitals.

cluster metal orbitals (−26, −17.3, and 34 eV, respectively). The second is significantly affected by bonding with the cluster, however.

Correlation of the cluster orbitals on interaction with the important C_2 fragment orbitals is shown in the center of Figure 6. The antibonding counterparts all lie well above the b_{1u} HOMO, starting with a_{2u}^* at −6.27 eV. Reduced overlap populations give useful measures of relative bond strengths, and a summary of these according to symmetry and metal atom type is given in Table VI.

The energy displacements shown in Figure 6, the observed scandium–carbon distances (Table III), and the overlap populations (Table VI) all reflect strong bonding between the cluster and the dicarbon unit via four orbital types on the latter. The π (e_u) orbitals on dicarbon are relatively effective in bonding with equatorial metal in the cluster, in spite of the lesser energy change produced. Actually, the inclusion of iodine functions produces two more near-lying e_u states with less carbon content that also contribute to this overlap population. Interaction between π^* orbitals on dicarbon and the cluster (e_g) is obviously energetically effective (Figure 6) and also produces the largest total overlap contribution (Table VI). The bonding utilizes metal d_{xz}, d_{yz} orbitals not only on the waist Sc(2)–Sc(5) (Figure 1) but also in significant amount on the axial metal atoms, as shown in **1** for

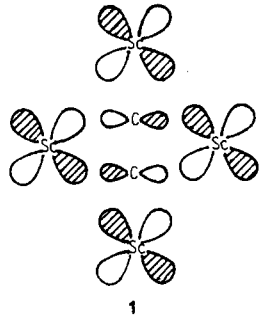

1

one of the two sets. The axial part is analogous to the traditional back-donation from electron-rich metal atoms into π-acceptor ligands in complexes.

The two remaining bonding MO's are σ in character and are of major importance in the remarkably tight bonding between axial scandium and the ends of the dicarbon, a_{1g} (shown) and a_{2u} at −17.9 eV. The former originates with the σ "s–p hybrid" bonding orbital on the C_2 fragment although a significant redistribution occurs on addition of axial scandium (and iodine). The magnitude of the overlap population deriving from the low-lying σ_s^* "lone-pair" orbital of dicarbon is actually more than twice as great as for the above a_{1g} MO in spite of the large energy separation between the fragment a_{2u} components in the cluster (−7.94 eV) and in the isolated dicarbon (−17.31 eV). The latter is lowered by 0.60 eV while the antibonding a_{2u} orbital is pushed up by over 1.6 eV. In fact, two additional bonding a_{2u} orbitals at −18.1 and −18.7 eV contribute 38% of the total Sc–C_2 population. The favorable disposition of the lone pair in this state is obviously important, and the opposite is true for σ_p.

The HOMO in $Sc_6I_{11}C_2$ is the half-occupied b_{2g} level, consistent with the magnetic properties (Figure 3). This level contains no carbon component and is metal–metal bonding mainly for equatorial scandium, as shown in **2**. This alone contributes 42%

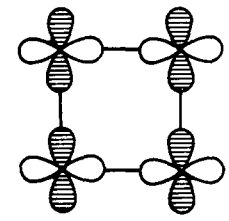

2

of the relatively small metal–metal overlap population total in the cluster, 0.370. The metal–metal components in the π^* (e_g) combinations **1** contribute another 36% as they are of the right symmetry and have significant overlap. Although the cluster equator involves relatively short Sc–Sc separations, it would seem that these and the cluster size in general depend much more on the dimensional requirements of the cluster–dicarbon bonding than on the strength of metal–metal bonding.

The charge distribution deduced from the calculations is +1.18 for each of the four equatorial scandium atoms, +1.08 for each axial metal atom, and −3.92 for the dicarbon. The first would be +1.42 without occupation of the metal–metal bonding HOMO, appropriately greater than for the more tightly bound axial metal atom, +1.08. Of course, the EHMO method is generally recognized to overestimate such charges. Furthermore, the valence-state energies in C_2 will rise when the effect of charge on the H_{ii} values for carbon is included. This change will serve to increase both the strength of the interaction of the lower lying states on the C_2 fragment with the cluster and the metal content of the bonding states and to cause the charges on both scandium and carbon to move toward zero. Thus, the charge on C_2 would become more similar to the values of −2.4 and −2.0 deduced for C_2 in gadolinium clusters.[18,19] Although the metal–carbon bonding is certainly somewhat polar in these compounds, a significant covalence is evident from the results, and it is difficult to understand the earlier conclusion that the bonding in the related $Gd_{10}Cl_{18}(C_2)_2$ is "predominantly ionic".[18]

A noteworthy and evidently general feature of the bonding of dicarbon in clusters is the presence of short and therefore presumably strong bonds to axial metal, although this feature has not been addressed before. In $Sc_6I_{11}C_2$ the two axial Sc–C interactions produce distances 0.26 Å shorter than the eight achieved between atoms in C_2 and the surrounding equatorial metal atoms, or 0.22 Å less than in the more symmetric monocarbide Sc-($Sc_6I_{12}C$).[3] Likewise, the Sc–C_2 overlap population for the equatorial system in $Sc_6I_{11}C_2$, 0.363 per metal, each with *two* carbon neighbors, is only 63% of the value for each axial Sc–C bond, 0.576. As seen in Table VI, this comes largely not just from σ bonds from σ_p and σ_s^* states of C_2 but also from the e_g (π^*) bonding, and the strong bonding is achieved in the presence of the short axial Sc–I^a bonds and the resulting competition for metal orbitals, largely in a_{1g}. The contrast between axial and equatorial bonding of C_2 in $Gd_2Br_2C_2$, $Gd_{10}Cl_{18}C_4$, and $Gd_{10}Cl_{17}C_4$ is in fact even greater, judging from the 0.32–0.34 Å difference between averages of the two types of Gd–C distances. Given this and the calculational results for both the scandium and gadolinium compounds, we are unable to follow the earlier conclusion that particularly strong axial bonding of gadolinium to C_2 is *not* supported by those data.[18]

The shortening of the axial M–C distances to C_2 relative to that about the π system appears to be a general feature of compounds in the CaC_2 structure type as well, which can be viewed in terms of similar but highly condensed $M_{6/6}C_2$ clusters. The differences in M–C bond lengths in these range between 0.22 and 0.25 Å for CaC_2, the rare-earth-metal dicarbides, and $UC_{1.86}$,[23,24] all examples

(23) Atoji, M. *J. Chem. Phys.* **1961**, *35*, 1950.

Table VII. Average Distances and Total Reduced Overlap Populations by Bond Type in the $Sc_6I_{11}C_2$ and $Sc_7I_{12}C$ Structures

	Sc(eq)	C	I^i	I^a
Distances (Å)				
		$Sc_6I_{11}C_2$		
Sc(eq) (×4)	3.16 (4)[a]	2.34 (8)	2.86 (8) 2.99 (8)	3.47 (4)
Sc(ax) (×2)	3.56 (8)	2.08 (2)	2.90 (8)	3.08 (2)
av	3.42			
		$Sc_7I_{12}C$[b]		
Sc	3.23 (9) 3.32 (3)	2.30 (6)	2.92 (24)	3.44 (6)
av	3.25			
Overlap Populations[c]				
	Sc(eq)	C	I^i	I^a
		$Sc_6I_{11}C_2$		
Sc(eq)	0.194 (4)[a]	1.45 (8)	8.54 (16)	0.497 (4)
Sc(ax)	0.176 (8)	1.15 (2)	3.04 (8)	0.608 (2)
tot.	0.370	2.61	11.58	1.105
		$Sc_7I_{12}C$		
Sc	1.01 (12)	2.06 (6)	8.30 (24)	0.817 (6)

[a] The number of contributing bonds or pairwise interactions is given in parentheses. [b] Reference 3. [c] The sum $c_ic_jS_{ij}$ over all occupied orbitals.

in which there are insufficient electrons to fill the π^* states.

The occurrence of dicarbon in clusters formed by such a small metal as scandium might seem unusual. The metallic radius of scandium is 0.16 Å less than that of gadolinium,[22] so the cavity provided for the same amount of metal–metal bonding is correspondingly smaller with scandium or, for the same size interstitial, the metal–metal bonding must be relatively less. However, we have seen that the metal–metal bonding contributions in $Sc_6I_{11}C_2$ are relatively small and unimportant compared with those of metal–carbon. Actually more surprising is the formation of the monocarbide in $Sc(Sc_6I_{12}C)$ with such a large anion and small metal core. In fact, a conflict between the bonding requirements of the small interstitial and the large matrix effect from iodide (or bromide) can be imagined to be responsible for the significant distortion of the cluster ($D_{3d} \rightarrow C_{3v}$), this allowing shorter and more nearly normal distances for the dominant Sc–C bonding while retaining 75% of the normal Sc–Sc distances within the cluster.[3] The distortion could also be electronically driven since the cluster carbide is a 13e species. A matrix effect is evidently not such a problem with chloride either in clusters like $Sc(Sc_6Cl_{12}(B,N))$ or in $Sc_4Cl_6(B,N)$, where elongation of the condensed clusters along the chain is prominent ($\sim D_{2h}$).[1]

Any attempt to understand further the differences in bonding between $Sc_6I_{11}C_2$ and $Sc(Sc_6I_{12}C)$ must allow for a diversity of Sc–Sc, Sc–C, and Sc–I distances in the two phases as well as for an increased number of carbon interactions in the former. Overlap populations in bonding orbitals weigh these apparent interactions much more appropriately than the easy simplicity of mentally relating interatomic distances to some inverse function of bond strength. Table VII provides a recapitulation of average "bond" distances in $Sc_6I_{11}C_2$ and $Sc(Sc_6I_{12}C)$ by Sc–Sc, Sc–C, Sc–I^i, and Sc–I^a interaction types and then compares the total overlap populations for these in the same way. This imaginary formation of the dicarbide from the monocarbide cluster involves some sizable changes in bonding (including in dicarbon) as well as two more bonding electrons, but it should be understood that we are by no means looking at all of the important terms in a complete thermochemical cycle.

As might be expected, the dicarbon cluster contains significantly less Sc–Sc bonding, the population decreasing from 1.11 to 0.370 not just because of the necessary axial expansion but also because of large reduction in the number of electrons present in the metal-based HOMO, which changes from t_{2g}^5 to b_{2g}^1. The difference effectively appears in more and stronger Sc–C bonds as reflected in a 30% gain in that overlap population. The axial atom bonding is an impressive fraction of that (Table VI). As far as Sc–I interactions, both calculations were carried out on $(Sc_6I_{12}Z)I_6^{n-}$ clusters of appropriate dimensions so the number of Sc–I "bonds" are the same. Marginal shortening of Sc–I^i distances both about the equator and for axial metal atoms (where there is less matrix effect and better overlap) and of Sc(axial)–I^a distances in the dicarbide produce an overall increase in these populations of about 40%. The persistence of $Sc_6I_{11}C_2$ under varying synthetic conditions is consistent with the above observations.

Simon[7,11] has prevented convincing evidence for the occurrence of the C_2 unit only for gadolinium halide compositions that provide seven or fewer additional electrons for bonding of neutral C_2 within the cluster after the halide levels are filled. Thus, known examples with between four and six electrons in this role show a parallel increase of d(C–C) of almost 0.2 Å as electrons are formally added to levels originating with the π^* states, while the seventh electron occupies a metal–metal-bonding state analogous to that found here in b_{2g}. However, it will be noted that the present $Sc_6I_{11}C_2$ with seven electrons beyond C_2 has a carbon–carbon distance 0.08 Å (but only 3σ) *less* than the maximum observed with gadolinium examples; this may relate to differences in the strength of the bonding to the cluster, particularly in the axial C_2–M interaction. It was presumed earlier that the presence of eight or more electrons would lead to occupation of the σ_p^* level of dicarbon and thereby give instability and the formation of monocarbide clusters such as in R_2Cl_2R, R = Sc, Y, Gd, Zr, etc., where four or more electrons are available per carbon. In terms of Figure 6, electrons beyond the six necessary to occupy the π^* state e_g will actually occupy first the bonding b_{2g} and then the slightly antibonding b_{1u} etc. levels, while σ_p^* lies much higher. Although the 4e/C limit does not describe a sufficient condition for the formation of monocarbide, this is probably too literal an interpretation. A more apt requirement for monocarbide formation is the availability of at least four electrons from the metal to fill both the carbon s and carbon p bands, the latter lying 3–5 eV below the HOMO (or E_F).[25]

Finally, it should again be noted that our interpretations of bonding and, in particular, stabilities as a function of interstitial, halide etc., necessarily depend on what researchers have been able to synthesize and characterize. Thus, missing compounds may arise not because they are inherently unstable but because the right set of synthetic conditions has not been found.

Acknowledgment. We are indebted to R. A. Jacobson for continued use of the X-ray and computing facilities, to R. N. Shelton for the magnetic results, and to T. R. Hughbanks for assistance and advice on the extended Hückel calculations. The research was supported by the National Science Foundation—Solid State Chemistry—under Grant DMR-8318616 and was carried out in the facilities of Ames Laboratory, DOE. The writing of this article was accomplished in part while J.D.C. was on leave at the Max-Planck-Institut für Festkörperforschung, Stuttgart, BRD, under the auspices of the Alexander von Humboldt-Stiftung, Bonn, BRD. This author is indebted to Professors H.-G. von Schnering and A. Simon in this respect.

Supplementary Material Available: Tables of anisotropic thermal parameters for and angles in $Sc_6I_{11}C_2$ and $Sc_4I_6C_2$, I–I distances in $Sc_6I_{11}C_2$, and parameters and coordinates used for the EHMO calculations (12 pages); tables of observed and calculated structure factors (13 pages). Ordering information is given on any current masthead page.

(24) Atoji, M. *J. Chem. Phys.* **1967**, *47*, 1188.

(25) Ziebarth, R. P.; Hwu, S.-J.; Corbett, J. D. *J. Am. Chem. Soc.* **1986**, *108*, 2594.